THE JOURNAL OF PHYSICAL CHEMISTRY A
A JOURNAL OF THE AMERICAN CHEMICAL SOCIETY

pubs.acs.org/JPCA

Article

# First-Principles Investigation of the Optical Properties of Eumelanin Protomolecules

Roberto Cardia, Nicolas Dardenne, Guido Mula, Elisa Pinna, Gian-Marco Rignanese, Jean-Christophe Charlier, and Giancarlo Cappellini*

Cite This: *J. Phys. Chem. A* 2023, 127, 10797−10806

Read Online

ACCESS | Metrics & More | Article Recommendations

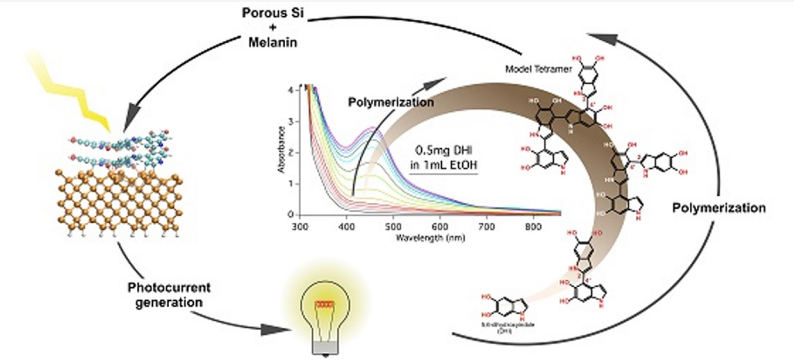


**ABSTRACT:** Using first-principles calculations, we investigate the absorption spectra (in the near-infrared, visible, and first UV range) of the two most probable eumelanin tetrameric molecules exhibiting either a linear open-chain or a cyclic porphyrine-like configuration. In order to simulate a realistic molecular system, an implicit solvent model is used in our calculations to mimic the effect of the solvated environment around the eumelanin molecule. Although the presence of solvent is found not to significantly affect the absorption pattern of both molecules, the onset of the spectra are shifted toward higher energies, especially for the linear tetramer. Interestingly, the absorption spectra and optical onsets of the two molecules differ significantly both in a vacuum and in ethanol. However, the two predicted spectra do not allow us to definitely discriminate between the two configurations when comparing the theoretical predictions with the available experimental spectrum. In addition, a mix of the two eumelanin configurations (close to fifty-fifty) leads to a maximum overlap between theoretical and experimental spectra. Consequently, this theoretical research shows that deeper insight can be gained using beyond DFT techniques on the real form of eumelanin protomolecules present in living systems as well as on their possible use in hybrid solar cells.

## INTRODUCTION

Melanin is the most common biological pigment present in living organisms in which it has several functions, mainly, thermoregulation, body exposed parts (skin, hair, eyes) coloration, and most importantly, photoprotection against UV radiation (is the cause of the suntan).[1−4]

In terms of chemical and physical behavior melanin presents several interesting properties[5] such as photoconductivity,[6−9] hydration-dependent electrical conductivity (in particular in the condensed phase),[6−10] metal-binding affinity (chelation), antioxidant behavior, free radical scavenging[6−9] and (consistently with its well-known photoprotectant role) an efficient nonradiative energy dissipation with the ability to deactivate UV and visible photon energy with radiative quantum yields < 0.05%.[10−13]

Melanin is well-known for its broadband IR-visible-UV absorption which presents a monotonic increase as the photon energy rises.[14] These peculiar characteristics have recently generated considerable interest in the possible use of synthetic melanin as a biomimetic functional soft material in applications such as biointerfaces,[15,16] hybrid materials,[17] energy storage,[6] and obviously (due to the conducting and absorption properties) organic electronics[2] and solar energy harvesting.[2,4,7,9,18−22] The latter is most probably the field that would benefit the most from employing natural or synthetic eumelanin (or their derived pigments) which could be used as a photoactive layer in hybrid solar cells.[18] Thanks to its

**Received:** July 20, 2023
**Revised:** November 27, 2023
**Accepted:** November 28, 2023
**Published:** December 18, 2023





https://doi.org/10.1021/acs.jpca.3c04898
*J. Phys. Chem. A* 2023, 127, 10797−10806

broad and continuous absorption spectrum, eumelanin has a high capability of capturing photons, and hence it could help to reach and possibly overcome the 10% efficiency obtained for some hybrid solar cells.[23]

This scenario leads to the need of performance assessment of eumelanin-based solar cells and, as a consequence, to the strong request of a deeper and refined theoretical analysis of materials and compounds used to build the devices. More specifically, it is extremely important to understand the exact form of eumelanin protomolecules and the interface effects between the photoactive material and the other materials in the cell and their consequences on the charge separation.

Despite the uncertainty associated to the exact atomic structure (mainly due to its adverse chemical and physical properties such as low solubility in most common solvents, difficulty in separation by chromatography, and opacity[24,25]), there is large consensus that, at the primary structural level, eumelanin is essentially composed of a set of different elementary molecules like 5,6-dihydroxyindole (DHI), 5,6-dihydroxyindole-2-carboxylic acid (DHICA), hydroquinone, semiquinone, quinone methide, and various quinone and DHI oxidized forms, which constitute its elementary building blocks.[26] Each of these molecules is characterized by a specific and quite narrow spectrum.[2,27−29]

Following the classification explained in refs 5, 10, and 30, several levels can be identified for the so-called "chemical disorder". At the lowest level, the elementary building blocks, namely, the monomers, may present some disorder. The latter is related to the variety of monomer building blocks contributing to the polymerization process. Then, comes the so-called size disorder that stems from the gathering of oligomers with gradually increasing complexity as a function of the level of local polymerization. At the next level, there is molecular disorder that describes the degree of structural diversity based on the variety of scaffolds. Then, arrives the electronic disorder that relates to the distribution of redox states (i.e., catechol, semiquinone, or quinone) within the oligomeric scaffold. Finally, at the highest level, arrives the supramolecular disorder which depends on the variety of aggregates that can be generated by intermolecular interactions, for example, $\pi$-stacking interactions (DHI units) or bundling aggregations (DHICA units).

This chemical disorder model[5,10,30] explains the heterogeneity as arising from a diversity in chemical structures, which differ in conjugation length, number of aromatic rings, and the redox state of the absorbing subunits. It also explains the absorption spectrum and excitation energy-dependent emission behavior of natural and synthetic eumelanins.[13,31]

Unfortunately, the chemical disorder model does not **identify** the exact identity of the actual absorbers (even if it is known that they are likely composed by the building blocks covalently bonded as mentioned above[32]), their organization in eumelanin larger macromolecules and/or stacks, or the way they interact.

The study of the spectrum of single possible eumelanin protomolecules could be useful to gain new information about the identity and the detailed structure of the actual absorber protomolecules. Our aim of this study is to gain new insight into the several absorbing subunits of natural and synthetic eumelanin.

There is a large number of possible candidates as eumelanin protomolecules (a rapid review of possible structures can be found in Chen et al.[19]).

Several experiments confirmed that eumelanin is made of stacked oligomers with an interlayer distance of 3−4 Å.[33,34] X-ray diffraction studies[35,36] and other measurements based on scanning tunneling microscopy (STM)[37−39] demonstrated that eumelanin protomolecules present a very small size (15−20 Å). This leads to the choice of tetramers of DHI and related oxidized forms covalently bonded as the most probable basic units of the large stacking and aggregates of eumelanin. In previous works the spectra of single monomers and of their stacked/bonded units have been considered.[40,41] Results for these systems and in this domain could be also found in other refs.[42−44]

A recent work of Antidormi et al.[20] shows that between several different forms of DHI tetramers, the two configurations proposed by Kaxiras et al.[45,46] and Panzella et al.[3] exhibit the better combination of formation energy and adhesion energy on the Si[001] surface.

For these reasons, and for additional motivations related to the previous results by some of the authors on this subject,[20,47] we decided to focus our attention on the linear open-chain molecule proposed by Panzella et al.[3] and the cyclic porphyrine-like structure proposed by Kaxiras et al.[45,46] as illustrated in Figure 1.

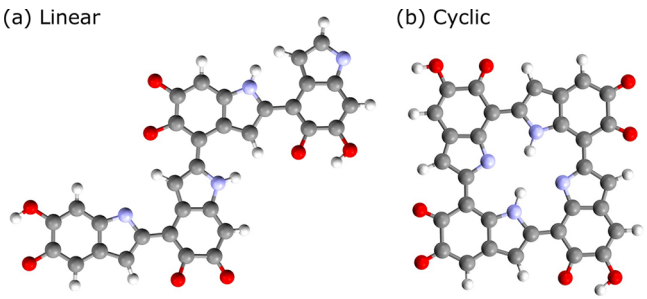


**Figure 1.** Linear open-chain (a) (left panel) and cyclic porphyrine-like (b) (right panel) eumelanin protomolecules considered in this work.

The low value of the formation energy implies that these structures are the most probable between the tetramerical structures analyzed in Antidormi et al.[20] The adhesion energy is one of the most important parameters in order to evaluate the possible use of the compound in a hybrid solar cell because it gives useful information about the stability of the interface between eumelanin tetramers and the Si[001] surface.

In the present work, Time Dependent Density Functional Theory (TDDFT) is used to calculate the absorption spectra of the above tetrameric eumelanin candidates in the range of near-IR, visible, and first UV. The results are validated by comparison with those calculated using Many Body Perturbation Theory (MBPT).

## COMPUTATIONAL METHODS

To determine the relaxed structures of the two configurations (linear and cyclic), DFT calculations are performed using the Gaussian 16[48] computational package. The structural relaxation is performed without imposing symmetry constraints using the M06-2X exchange-correlation (XC) functional[49,50] and the Aug-cc-pVDZ and (augmented, polarized double-$\zeta$) localized basis set.[51] The Berny geometry optimization algorithm[52] is used setting the RMS forces criterion to $10^{-5}$ eV/Å. We checked the basis set convergence by adopting the


https://doi.org/10.1021/acs.jpca.3c04898
J. Phys. Chem. A 2023, 127, 10797−10806

Aug-cc-pVTZ (augmented, polarized triple-$\zeta$) basis set,[51] but it turned out that the Aug-cc-pVDZ basis already provides a very good agreement with experiments. We would like to point out that, in previous calculations on other molecular systems carried by some of us,[47,53−64] it had been found that using the B3LYP XC functional[65,66] and the 6−31+G*basis set[67] was sufficient to obtain relaxed structures in good agreement with the corresponding experimental data, in particular for the eumelanin related precursors (DHI) and protomolecules.[21,22,68] In contrast, we find here that for systems like the tetrameric molecules of eumelanin such a level of theory (in terms of XC functional and basis set) leads to rather unsatisfactory results.

To determine the excitation energies and the electronic absorption spectra in the visible-near-UV regions, different approaches are considered. TDDFT calculations are first performed adopting the same levels of theory (M06-2X with Aug-cc-pVDZ and Aug-cc-pVTZ) used for the structural optimizations. More specifically, we adopt the Casida approach[69] based on the linear response of the density-matrix as implemented in the Gaussian 16 software package. Within this method, the poles of the linear response function correspond to vertical excitation energies ($E_i$), and their amplitudes are related to the oscillator strengths ($f_i$) of the transitions. For each molecule, we calculate 200 roots which cover an energy range up to 7.3−7.4 eV. To take into account the effects of the $C_2H_5OH$ (ethanol) solvent on the relaxed structure of the molecules and on their excitation properties, the DFT and TDDFT calculations (relying on the M06-2X XC functional with the Aug-cc-pVDZ basis set) are repeated adopting a density corrected Polarizable Continuum Model (PCM-SMD), which is an implicit solvent model.[70,71] The use of more advanced, but numerically more challenging methods to treat the molecule−solvent interaction,[72,73] are postponed to a future computational campaign.

Finally, many-body perturbation theory (MBPT) calculations are also performed within the *GW* and Bethe-Salpeter equation (BSE) formalisms[74−78] as implemented within the FIESTA package.[79−81] For a fair comparison with the TDDFT calculations, the Green's functions $G$ and the screened Coulomb potential $W$ are generated with the Gaussian 16 code using the same M06-2X exchange-correlation functional[49,50] and the Aug-cc-pVTZ basis set[51] as for the TDDFT calculations. Following a recent benchmark study of the optical absorption energies of a large standard set of organic molecules,[81] a partially self-consistent *GW* approach is adopted, namely, the corrected quasiparticle energies are reinjected self-consistently in the construction of the Green's function $G$ and the screened Coulomb potential $W$. This procedure leads to an excellent agreement with the "best theoretical estimates" provided by high-level quantum chemistry techniques, with a mean-absolute error of the order of 0.2 eV[81] and with errors in the calculation of singlet excitation energies of 0.1−0.2 eV.[78,82] Our BSE calculations are performed going beyond the Tamm-Dancoff approximation, namely mixing excitations and de-excitations as described in ref 81. The BSE calculations provide the discrete energies ($E_i$) and the corresponding oscillator strengths ($f_i$) for each founded excitonic state which can then be used to construct the absorption spectrum by convolution with Lorentzian curves (centered in $E_i$ and whose height is proportional to $f_i$) and their sum along the energy window explored. With this formalism, we consider the first active excitation (with nonzero oscillator strength) as the optical onset. Further details about the methodology can be found in refs 79−81.

## RESULTS AND DISCUSSION

In order to obtain a quantitative assessment of the resemblance between two absorption spectra $A_1(E)$ and $A_2(E)$, we define their overlap over the energy range $(0, E_M)$ as

$$\text{Overlap}(A_1, A_2) = \frac{\int_0^{E_M} \min[A_1(E), A_2(E)]\, dE}{\sqrt{\left[\int_0^{E_M} A_1(E)\, dE\right] \times \left[\int_0^{E_M} A_2(E)\, dE\right]}} \quad (1)$$

Using this mathematical trick, it is possible to determine the average shift $\Delta E$ from one absorption spectrum to another as the one that maximizes the overlap. Note that, in this maximization, a scaling factor can also be applied given that there is some arbitrariness on the intensity of the absorption spectra. In the end, the similarity between two $A_1(E)$ and $A_2(E)$ is characterized by the average shift $\Delta E$ and the overlap (expressed in %).

First of all, we check the convergence of the TDDFT calculations with respect to the basis set size. The Aug-cc-pVDZ and Aug-cc-pVTZ basis sets lead to very similar results. The overlaps between the absorption spectra are 91% and 97% for the linear and cyclic tetramers, respectively; and the average shifts $\Delta E$ are very small (0.00 and 0.08 for the linear and cyclic tetramer, respectively). Based on this observation, it seems very reasonable to perform all further calculations using the smaller basis set (Aug-cc-pVDZ) in order to limit the computational load for these rather large systems (58 atoms and 298 electrons for the linear tetramer and 56 atoms and 296 electrons for the cyclic one). So, from here on, we will refer to these calculations simply as TDDFT (without specifying the basis set anymore). It is worth mentioning that our TDDFT results are consistent with those from previous works. For example, our results in terms of energy excitations for the cyclic tetramer show 1−3% differences with respect to those of ref 83.

We now turn to the validation of the TDDFT calculations relying on the M06-2X XC functional. To this end, we compare them to MBPT calculations, which can be considered as a robust reference. Indeed, they have been shown to predict accurately charge-transfer excitations[80,84] and even cyanine-like transitions,[85] both known to be quite problematic for the typical TDDFT calculations. In Figure 2, we report the absorption spectra of the linear and cyclic tetramers calculated by using TDDFT (in red) and MBPT (in orange). The average shifts $\Delta E$ values are reported with respect to the absorption spectrum obtained in TDDFT.

The computed spectra look very much alike, with overlaps of 91% and 93% for the linear and cyclic tetramers, respectively. The corresponding average shifts $\Delta E$ are 0.14 and 0.20 eV from MBPT to TDDFT, respectively. In Table 1, we report the shifts $\delta E_i$ (eV) for the first eight prominent peaks. For each of them, if $\delta E_i < \Delta E$ (respectively $\delta E_i > \Delta E$), the MBPT peak will be seen higher (respectively lower) in energy than the TDDFT one in Figure 2. These results are in line with the typical 0.1−0.6 eV upward shift observed previously for other organic and biological compounds such as cyanine derivatives,[86] coumarins,[87] polycyclic aromatic hydrocarbons,[57] or porphyrinic molecules.[88]

In particular, it is worth comparing the onsets of the computed absorption spectra (the first peak in Figure 2) with



https://doi.org/10.1021/acs.jpca.3c04898
J. Phys. Chem. A 2023, 127, 10797−10806

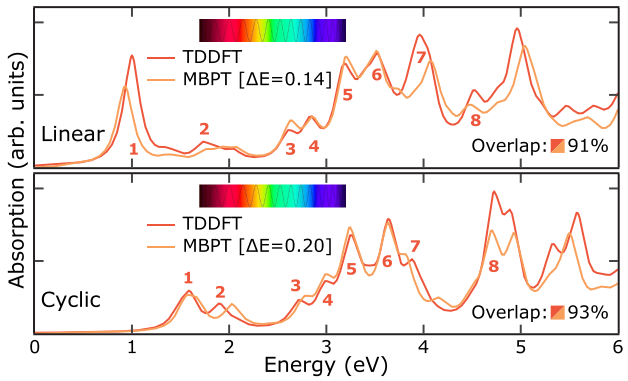


**Figure 2.** Absorption spectra of the linear tetramer (a) (upper panel) and cyclic tetramer (b) (lower panel) computed using TDDFT (in red) and MBPT (in orange). The TDDFT absorption spectrum is used as a reference for obtaining the average shifts $\Delta E$ and for expressing the overlaps. The visible region is highlighted in the plot.

respect to both their position and their origin in terms of electronic excitations. For the linear tetramer, the onset is at 0.99 and 0.79 eV within TDDFT and MBPT, respectively. The 0.20 eV difference is in the typical range observed in previous calculations.[86,87] It is a bit larger than the average shift between the two spectra ($\Delta E$ = 0.14 eV), which translates into a left shift in the first peak position in Figure 2. For both TDDFT and MBPT calculations, the onset absorption is basically dominated by a HOMO → LUMO transition. For the cyclic tetramer, the onset is located at 1.48 and 1.59 eV within TDDFT and MBPT, respectively. The 0.11 eV difference is a bit lower than the average shift between the two spectra ($\Delta E$ = 0.20 eV). This can be noticed in Figure 2 through the slight right shift in the first peak position. Just like for the linear tetramer, the main contribution to the onset originates from the HOMO → LUMO transition for both TDDFT and MBPT calculations.

As the TDDFT results seem perfectly valid with respect to the MBPT ones, the subsequent calculations are performed relying only on TDDFT.

**Solvent Effects.** Given that the experimental polymerization and absorption measurements for the eumelanin compounds studied here are typically performed in a solvated environment, solvent effects should also be accounted for in the calculation of the absorption spectra. It goes well beyond the scope of present work to tackle directly the problem of structural optimization and excited state calculation in the explicit presence of molecules of the solvent. Indeed, such simulations are extremely demanding due to the size of the molecules (56 and 58 atoms) and the amount of solvent molecules required to obtain an acceptable first solvation shell. As an example, it has been estimated that, for the cyclic porphyrine-like geometry, at least 400 solvent molecules are needed for a correct solvation.[83,89] This would represent an extremely heavy computational load in particular within the BSE that scales like $O(N^4)$.[90] For this reason, we resorted to the SMD-PCM[70,71] implicit solvent scheme, despite the fact that such models may have limitations in identifying the correct optical transitions in some organic pigments.[91] In Figure 3, the resulting spectra are compared to those obtained in vacuum.

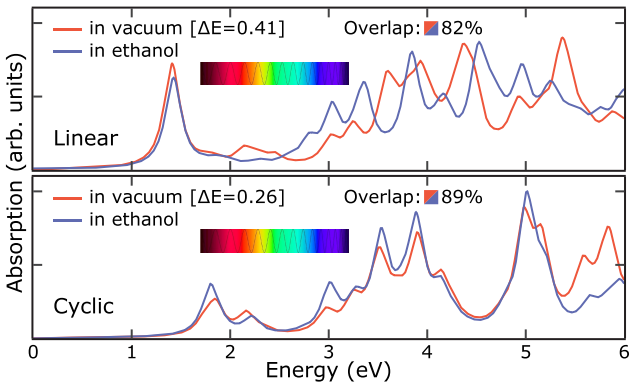


**Figure 3.** Absorption spectra of linear tetramer (a) (upper panel) and cyclic tetramer (b) (lower panel) computed using TDDFT in a vacuum (in red) and in ethanol (in blue). The absorption spectrum in a vacuum is used as a reference for obtaining the average shifts $\Delta E$ and for expressing the overlaps. The visible region is highlighted in the plot.

The overlaps between the absorption spectra are 82% and 89% for the linear and cyclic tetramers, respectively. These large overlaps indicate that the main effect of the solvent is to shift the spectrum by $\Delta E$ = 0.41 and 0.26 eV for the linear and cyclic tetramer, respectively. For the linear tetramer, the spectra are more similar in the range between 1 and 3 eV than for energies larger than 4 eV, where the individual peaks may change both in position and intensity. The first optical active transition (onset) is located at 1.43 eV with a shift $\delta$ of ~0.4 eV with respect to the calculation in vacuum. That is almost exactly the value of the average shift. The central large absorption structure consists of four peaks located at 3.03, 3.36, 3.84, and 4.16 eV with shifts $\delta$ of 0.42, 0.52, 0.65, and

**Table 1. Position $E_i$ (eV) of the Most Prominent Peaks of the Absorption Spectra of the Linear and Cyclic Tetramers Computed Using TDDFT and MBPT[a]**

| | Peak no. | 1 | 2 | 3 | 4 | 5 | 6 | 7 | 8 |
|---|---|---|---|---|---|---|---|---|---|
| | | | | Linear | | | | | |
| TDDFT | $E_i$ (eV) | 1.00 | 1.73 | 2.60 | 2.83 | 3.19 | 3.52 | 3.96 | 4.52 |
| MBPT | $E_i$ (eV) | 0.79 | 1.62 | 2.50 | 2.71 | 3.07 | 3.37 | 3.93 | 4.33 |
| | $\delta E_i$ (eV) | 0.21 | 0.11 | 0.10 | 0.12 | 0.12 | 0.15 | 0.03 | 0.19 |
| | | | | Cyclic | | | | | |
| TDDFT | $E_i$ (eV) | 1.58 | 1.90 | 2.72 | 2.99 | 3.26 | 3.64 | 3.88 | 4.73 |
| MBPT | $E_i$ (eV) | 1.38 | 1.83 | 2.59 | 2.80 | 3.05 | 3.43 | 3.60 | 4.49 |
| | $\delta E_i$ (eV) | 0.20 | 0.07 | 0.13 | 0.19 | 0.21 | 0.21 | 0.28 | 0.24 |

[a]The corresponding shifts $\delta E_i$ (eV) are also reported for each individual peak. These should be compared to the average shifts $\Delta E$ of 0.14 and 0.20 eV for the linear and cyclic tetramers, respectively.



https://doi.org/10.1021/acs.jpca.3c04898
J. Phys. Chem. A 2023, 127, 10797−10806

0.64 eV, respectively, with respect to the calculation in vacuum. While $\delta \simeq \Delta$ for the first peak, it is systematically bigger by 0.1−0.2 eV for the next three. Furthermore, their relative intensities of the peaks are quite different in vacuum and in ethanol.

The largest peak in terms of oscillator strength appears at 4.53 eV with a shift $\delta$ of 0.57 eV (that is 0.15 eV larger than $\Delta$). At higher energies, three other peaks are present at 4.97, 5.25, and 5.76 eV with shifts $\delta$ of 0.45, 0.29, and 0.29 eV, respectively, with respect to the calculation in vacuum. While $\delta \simeq \Delta$ for the first peak, $\delta \simeq \Delta$−0.13 eV for the two following, and their intensities vary considerably.

For the cyclic tetramer, the similarity is significantly larger. The peaks are basically shifted by values very close to $\Delta$ = 0.26 eV. The optical onset is located at 1.80 eV with a shift of $\delta$ = 0.22 eV with respect to the corresponding onset in vacuum. Like in the vacuum spectrum, there is a large and complex structure in the middle of the spectrum (between 2.5 and 4.5 eV) formed by five peaks. These are located at 3.02, 3.28, 3.53, 3.89, and 4.12 eV with shifts of 0.29, 0.29, 0.28, and 0.25 eV, respectively, with a small amplitude change in the first. The merged peaks at 5.02 and 5.21 eV (1 dominant + 1 shoulder) show a structure similar to that in the vacuum spectrum with shifts $\delta$ of 0.29 and 0.31 eV.

Globally, the presence of a solvent does not change the absorption spectrum dramatically. It mainly amounts to a shift of the spectrum with some reorganization in terms of amplitude, which is more important in the linear tetramer than in the cyclic one.

Figure 4 (top panels) shows the calculated spectra for both the tetramers with the experimental data from ref 21. Those absorption measurements were obtained for DHI polymers after completing the polymerization process as an example of synthetic eumelanin.

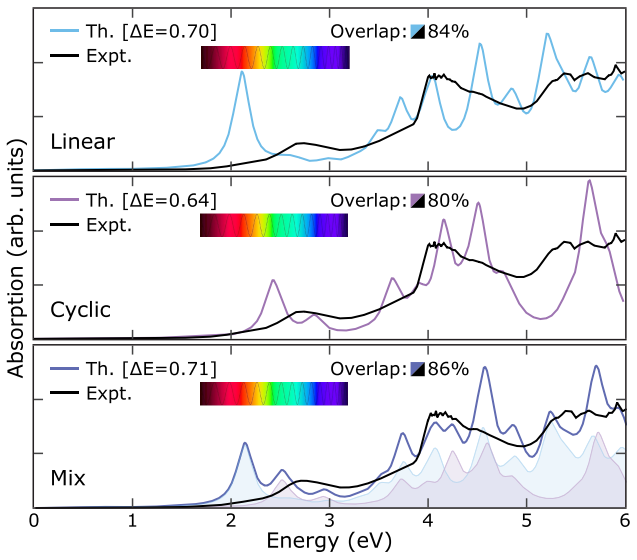


**Figure 4.** Absorption spectra of the linear tetramer (a) (in light blue, upper panel) and cyclic tetramer (b) (in purple, central panel) computed using TDDFT in ethanol, as well as of a mix of both (c) (in blue, lower panel), compared with the measured experimental spectrum of polymerized DHI/eumelanin (in black).[21] The experimental absorption spectrum is used as a reference for obtaining the average shifts $\Delta E$ and for expressing the overlaps. The visible region is highlighted in the plot.

Both calculated spectra show a large overlap with the experimental data (84% and 80% for the linear and cyclic tetramers, respectively). Interestingly, the average shifts at $\Delta$ = 0.70 and 0.64 eV are very similar, demonstrating the coherence of the predictions. The slight difference in overlap is not sufficient to assign the experiments to one of the two molecular configurations.

In fact, both calculated spectra present a number of mismatches with respect to the experimental data. The first main discrepancy is in the theoretical onset, which is located at 2.12 eV (respectively 2.44 eV) for the linear (respectively cyclic) tetramer, while it is measured at 2.72 eV experimentally. The discrepancy is particularly important for the linear tetramer, given that there is basically no absorption at 2.12 eV in the experimental spectrum. For the linear tetramer, the other important discrepancy is the presence of a dip at 4.24 eV that does not show up in experiments. Similarly, for the cyclic tetramer, an even more pronounced dip appears at 5.17 eV in a region where the absorption is rather important experimentally.

If we mix both calculated spectra, the maximum overlap reaches 86% using a unique average shift $\Delta$ = 0.71 eV while allowing for a different fraction of both tetramers (53% and 47% for the linear and cyclic tetramers, respectively). The corresponding spectrum is reported in the bottom panel of Figure 4, where the contributions of the linear and cyclic tetramers are also represented as shaded areas. Apart from the remaining discrepancy on the theoretical onset (though it is considerably smaller than for the individual tetramers), the agreement with the experimental data is very good. In particular, the two dips mentioned above have been filled by the absorption from the other tetramer. Interestingly, the average shifts for the individual tetramers and their mix are all very similar (with at most 0.07 eV difference).

Finally, it is important to recall that the experimental results are obtained based on a set of measurements on DHI solutions prepared using a given mass of DHI monomer dissolved into ethanol. The time variation of the absorption spectrum of the solution shows that there is a multistep evolution of the solution composition when the DHI monomers start to aggregate to form a variety of oligomers. As discussed in ref 21, the different temporal behavior of the peaks visible at different wavelengths indicate that the composition changes in a complex way over time, with the presence of different oligomers whose relative composition also varies over time. For this reason, while the study of the solution absorption over time is a powerful tool to study the evolution of the solution composition (with spectra taken in ethanol solution starting from DHI powder as a function of time; see ref 21), the superposition of the spectral responses makes it difficult to unambiguously identify the unique optical response of each kind of molecule. Therefore, the remaining differences between the theoretical and experimental spectra could be ascribed to the different levels and mechanisms of chemical disorder taking place during the polymerization.

As a final comment, it is known from previous works[60,91] that a calculation with an explicit solvent could lead to a blue shift with respect to the implicit solvent spectrum. This was observed both within TDDFT[91] and MBPT[60] for natural dyes and, more generally, for functionalized organic molecules. This blue shift has been ascribed to the presence of higher order solvation effects, such as those caused by the explicit solvent shell around the tetramers. As a possible future development, it


https://doi.org/10.1021/acs.jpca.3c04898
J. Phys. Chem. A 2023, 127, 10797−10806

might be interesting to include explicit solvent effects in the calculation of the spectra for the two eumelanin tetramers.

## ■ ADDITIONAL COMPUTATIONAL RESULTS

In order to give additional chemical information relative to the details of the transitions involved in the studied spectra, we report here the additional data in Table 2.

**Table 2. Main Transitions for Optical Onset and Main Absorption Structure for Linear and Cyclic Melanin Tetramer in Gas Phase and under Implicit Solvation (Ethanol)**

| molecule | peak | energy [eV] | transitions | O.S. |
|---|---|---|---|---|
| linear | peak 1 (onset) | 1.00 | H → L (0.51) | 0.50 |
| | | | H → L+4 (0.35) | 0.31 |
| | | | H−2 → L+3 (0.28) | |
| | peak 7 (main) | 3.96 | H → L+4 (0.42) | 0.25 |
| | | | H−9 → L (0.25) | |
| cyclic | peak 1 (onset) | 1.58 | H → L (0.50) | 0.29 |
| | | | H → L+1 (0.32) | |
| | peak 8 (main) | 4.73 | H → L+4 (0.49) | 0.62 |
| | | | H−10 → L (0.38) | |
| linear ethanol | peak 1 (onset) | 1.70 | H → L (0.40) | 0.50 |
| | | | H → L+1 (0.24) | |
| | peak 7 (main) | 4.00 | H → L+4 (0.45) | |
| | | | H−7 → L (0.22) | 0.52 |
| cyclic ethanol | peak 1 (onset) | 2.25 | H → L (0.63) | |
| | | | H−1 → L+1 (0.18) | 0.37 |
| | peak 7 (main) | 5.43 | H → L+4 (0.52) | 0.93 |
| | | | H−10 → L (0.36) | |

Moreover we also added the plots of the molecular frontier orbitals corresponding to the dominant transition for the optical onset in the case of linear (Figure 5) and cyclic (Figure 6) molecules.

Considering the data reported in Table 2, one can obtain a clearer picture on which transitions have the leading position in the composition of the two structures. We would like to focus in the absorption spectra, i.e., the onset peak and the main peak in the energy range here studied. From the data in this table it is clear that the nature of the transitions involved changes with respect to the two studied cases, i.e., molecule in vacuum or in ethanol. Considering the linear molecule aside from the shift for the onset energy we have discussed previously, there is a change in the transitions involved: for this onset energy, aside from the transition from H to L with similar probability, in the ethanol case the transition from H to L+1 takes place in substitution to the two transitions from H to L+4 and from H−2 to L+3. The main peak for this molecule does not show a large modification (shift of the order of 1%) in its energy position, and the transition from H to L+4 results as the strongest for the molecule in vacuum and in ethanol. A modification occurs for the lower rank contribution for this peak, which goes from the H−9 to L transition in the vacuum case to the H−7 to L transition for the case in ethanol. In the case of the cyclic tetramer, the onset peak has the H to L transition in both cases (vacuum and ethanol) as the principal contribution. In addition to that there is a contribution from H to L+1 for the case in a vacuum and H−1 to L+1 for the case in ethanol. For the strongest peak in the absorption curves, aside from a larger effect of the solvent in its energy position (shift around 14%), the main transition either for the vacuum and for the ethanol case remains the H to L+4 one. Moreover in both cases (vacuum and ethanol), the following transition in importance is the H−10 to L one. From Table 2 and the above discussion it is clear that the HOMO and LUMO orbitals play a fundamental role in the transitions composing both the onset and the main peak for both the molecules. Therefore we reported in the linear and cyclic tetramer the spatial representations of those orbitals for the two molecules under study. It is clear from those figures that the linear eumelanin tetramer shows a different distribution of the HOMO and LUMO orbitals with respect to the cyclic case. In fact it is clear from Figure 5 that the HOMO orbitals occupy a part of the molecule which is nearly free in the case of the LUMO state: this means that in this case the HOMO−LUMO transition could give rise to a charge-transfer exciton. On the other hand it is clear from Figure 6 that this is not the case for the cyclic molecule in which the lobes in the HOMO and in the LUMO case does not show particular charge localization.[92]

## ■ CONCLUSIONS

First-principles calculations have been used to investigate the near-infrared, visible, and first UV absorption spectra of two of the most important candidates as eumelanin chromophores. The first one is characterized by a linear open-chain geometry, and the second one by a cyclic porphyrine-like structure.

The TDDFT results are first validated by comparison with those from MBPT. Similar to other organic/biological molecules, those two optical spectra do not show important differences for both compounds. More precisely, the MBPT spectra are basically red-shifted by a few tenths of an eV compared to the TDDFT ones. The presence of ethanol as a solvent is then investigated by adopting an implicit PCM-SMD

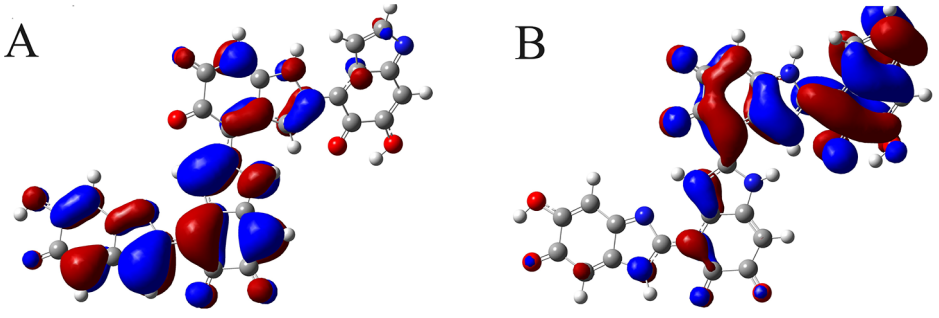


**Figure 5.** Highest occupied molecular orbital (HOMO) [(a) (left panel)] and lowest unoccupied molecular orbital (LUMO) [(b) (right panel)] for the linear open-chain eumelanin protomolecule (gas phase).



https://doi.org/10.1021/acs.jpca.3c04898
J. Phys. Chem. A 2023, 127, 10797−10806

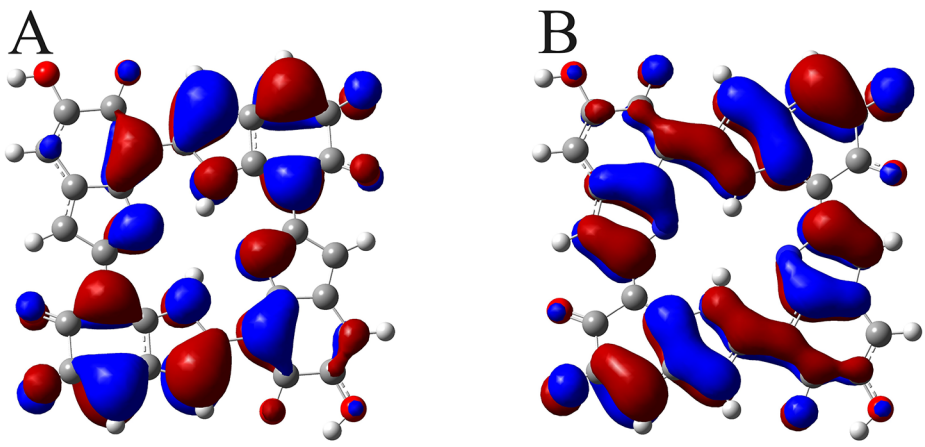


**Figure 6.** Highest occupied molecular orbital (HOMO) [(a) (left panel)] and lowest unoccupied molecular orbital (LUMO) [(b) (right panel)] for the cyclic eumelanin protomolecule (gas phase).

solvation model in the TDDFT calculations. Compared with the TDDFT results in vacuum, a small blueshift of the spectrum (0.3−0.4 eV) is observed without significant modifications of the main absorption features for both tetramers.

The comparison of the calculated result with a previously measured experimental spectrum does not allow for a clear statement about which tetramer is the most likely. In fact, both tetramers show a very good agreement with experiments, and a mix of both of them leads to an even more significant theory−experiment accordance, with a slightly higher fraction of linear tetramer. The present results, obtained using state of the art simulation techniques, can help to obtain deeper insight into the exact configuration of eumelanin protomolecules. This issue can have important consequences with respect to either basic or applied research involving eumelanin.

## ■ ASSOCIATED CONTENT

### Data Availability Statement

Data will be made available on request.

## ■ AUTHOR INFORMATION

### Corresponding Author

**Giancarlo Cappellini** − *Department of Physics, Università degli Studi di Cagliari, Cittadella Universitaria, I-09042 Monserrato, Cagliari, Italy; European Theoretical Spectroscopy Facility (ETSF);* orcid.org/0000-0001-9746-3025; Email: giancarlo.cappellini@dsf.unica.it

### Authors

**Roberto Cardia** − *Department of Physics, Università degli Studi di Cagliari, Cittadella Universitaria, I-09042 Monserrato, Cagliari, Italy*

**Nicolas Dardenne** − *Institute of Condensed Matter and Nanosciences, Université catholique de Louvain (UCLouvain), B-1348 Louvain-la-Neuve, Belgium*

**Guido Mula** − *Department of Physics, Università degli Studi di Cagliari, Cittadella Universitaria, I-09042 Monserrato, Cagliari, Italy*

**Elisa Pinna** − *Department of Physics, Università degli Studi di Cagliari, Cittadella Universitaria, I-09042 Monserrato, Cagliari, Italy*

**Gian-Marco Rignanese** − *Institute of Condensed Matter and Nanosciences, Université catholique de Louvain (UCLouvain), B-1348 Louvain-la-Neuve, Belgium; European Theoretical Spectroscopy Facility (ETSF);* orcid.org/0000-0002-1422-1205

**Jean-Christophe Charlier** − *Institute of Condensed Matter and Nanosciences, Université catholique de Louvain (UCLouvain), B-1348 Louvain-la-Neuve, Belgium; European Theoretical Spectroscopy Facility (ETSF)*

Complete contact information is available at: https://pubs.acs.org/10.1021/acs.jpca.3c04898

### Notes

The authors declare no competing financial interest.

## ■ ACKNOWLEDGMENTS

All the authors acknowledge the use of the code FIESTA and the kind scientific collaboration with Xavier Blase of CNRS and Grenoble-Alpes University, Institut Néel. G.C acknowledges financial support from IDEA-AISBL, Bruxelles, Belgium and from CINECA through the ISCRA initiative, for the high-performance computing resources and technical support (ISCRA-C Project SolvSpec: "Solvent Effects on Absorption Spectra of Eumelanin Polymers"). J.-C.C. and G.-M.R. acknowledge financial support from the National Fund for Scientific Research [F.R.S.-FNRS] of Belgium. Computational resources have been provided by a PRACE project (No. 2016153610) and by the supercomputing facilities of the Université Catholique de Louvain (CISM/UCL) and the Consortium des Équipements de Calcul Intensif en Fédération Wallonie Bruxelles (CÉCI) funded by the Fond de la Recherche Scientifique de Belgique (F.R.S.-FNRS) under convention No. 2.5020.11.

## ■ REFERENCES

(1) Ito, S.; Wakamatsu, K.; d'Ischia, M.; Napolitano, A.; Pezzella, A. *Melanins and Melanosomes: Biosynthesis, Biogenesis, Physiological, and Pathological Functions*; John Wiley and Sons, Ltd, 2011; Chapter 6, pp 167−185.

(2) d'Ischia, M.; Napolitano, A.; Pezzella, A.; Meredith, P.; Sarna, T. Chemical and Structural Diversity in Eumelanins: Unexplored Bio-Optoelectronic Materials. *Angewandte Chemie International Edition* **2009**, *48*, 3914−3921.

(3) Panzella, L.; Gentile, G.; D'Errico, G.; Della Vecchia, N. F.; Errico, M. E.; Napolitano, A.; Carfagna, C.; d'Ischia, M. Atypical Structural and π-Electron Features of a Melanin Polymer That Lead to Superior Free-Radical-Scavenging Properties. *Angewandte Chemie International Edition* **2013**, *52*, 12684−12687.

(4) d'Ischia, M.; Napolitano, A.; Pezzella, A.; Meredith, P.; Buehler, M. Melanin Biopolymers: Tailoring Chemical Complexity for Materials Design. *Angewandte Chemie International Edition* **2020**, *59*, 11196−11205.
(5) Meredith, P.; Powell, B. J.; Riesz, J.; Nighswander-Rempel, S. P.; Pederson, M. R.; Moore, E. G. Towards structure-property-function relationships for eumelanin. *Soft Matter* **2006**, *2*, 37−44.
(6) Xu, R.; Gouda, A.; Caso, M. F.; Soavi, F.; Santato, C. Melanin: A Greener Route To Enhance Energy Storage under Solar Light. *ACS Omega* **2019**, *4*, 12244−12251.
(7) Di Mauro, E.; Xu, R.; Soliveri, G.; Santato, C. Natural melanin pigments and their interfaces with metal ions and oxides: emerging concepts and technologies. *MRS Communications* **2017**, *7*, 141−151.
(8) Jastrzebska, M.; Kocot, A.; Tajber, L. Photoconductivity of synthetic dopa-melanin polymer. *Journal of Photochemistry and Photobiology B: Biology* **2002**, *66*, 201−206.
(9) Meredith, P.; Bettinger, C. J.; Irimia-Vladu, M.; Mostert, A. B.; Schwenn, P. E. Electronic and optoelectronic materials and devices inspired by nature. *Rep. Prog. Phys.* **2013**, *76*, No. 034501.
(10) Tran, M. L.; Powell, B. J.; Meredith, P. Chemical and Structural Disorder in Eumelanins: A Possible Explanation for Broadband Absorbance. *Biophys. J.* **2006**, *90*, 743−752.
(11) Huijser, A.; Pezzella, A.; Sundström, V. Functionality of epidermal melanin pigments: current knowledge on UV-dissipative mechanisms and research perspectives. *Phys. Chem. Chem. Phys.* **2011**, *13*, 9119−9127.
(12) Gauden, M.; Pezzella, A.; Panzella, L.; Neves-Petersen, M. T.; Skovsen, E.; Petersen, S. B.; Mullen, K. M.; Napolitano, A.; d'Ischia, M.; Sundström, V. Role of Solvent, pH, and Molecular Size in Excited-State Deactivation of Key Eumelanin Building Blocks: Implications for Melanin Pigment Photostability. *J. Am. Chem. Soc.* **2008**, *130*, 17038−17043.
(13) Meredith, P.; Riesz, J. Radiative Relaxation Quantum Yields for Synthetic Eumelanin. *Photochem. Photobiol.* **2004**, *79*, 211−216.
(14) Kohl, F. R.; Grieco, C.; Kohler, B. Ultrafast spectral hole burning reveals the distinct chromophores in eumelanin and their common photoresponse. *Chem. Sci.* **2020**, *11*, 1248−1259.
(15) Bettinger, C. J.; Bruggeman, J. P.; Misra, A.; Borenstein, J. T.; Langer, R. Biocompatibility of biodegradable semiconducting melanin films for nerve tissue engineering. *Biomaterials* **2009**, *30*, 3050−3057.
(16) Pezzella, A.; Barra, M.; Musto, A.; Navarra, A.; Alfe, M.; Manini, P.; Parisi, S.; Cassinese, A.; Criscuolo, V.; d'Ischia, M. Stem cell-compatible eumelanin biointerface fabricated by chemically controlled solid state polymerization. *Mater. Horiz.* **2015**, *2*, 212−220.
(17) Prasetyanto, E. A.; Manini, P.; Napolitano, A.; Crescenzi, O.; d'Ischia, M.; De Cola, L. Towards Eumelanin Zeolite Hybrids: Pore-Size-Controlled 5,6-Dihydroxyindole Polymerization. *Chem.-Eur. J.* **2014**, *20*, 1597−1601.
(18) McGehee, M. D. Nanostructured Organic-Inorganic Hybrid Solar Cells. *MRS Bulletin* **2009**, *34*, 95−100.
(19) Chen, C.-T.; Chuang, C.; Cao, J.; Ball, V.; Ruch, D.; Buehler, M. J. Excitonic effects from geometric order and disorder explain broadband optical absorption in eumelanin. *Nature Communications* **2014**, *5*, 3859.
(20) Antidormi, A.; Melis, C.; Canadell, E.; Colombo, L. Assessing the Performance of Eumelanin/Si Interface for Photovoltaic Applications. *The Journal of Physical Chemistry C* **2017**, *121*, 11576−11584.
(21) Pinna, E.; Melis, C.; Antidormi, A.; Cardia, R.; Sechi, E.; Cappellini, G.; d'Ischia, M.; Colombo, L.; Mula, G. Deciphering Molecular Mechanisms of Interface Buildup and Stability in Porous Si/Eumelanin Hybrids. *International Journal of Molecular Sciences* **2017**, *18*, 1567.
(22) Antidormi, A.; Aprile, G.; Cappellini, G.; Cara, E.; Cardia, R.; Colombo, L.; Farris, R.; d'Ischia, M.; Mehrabanian, M.; Melis, C.; et al. Physical and Chemical Control of Interface Stability in Porous Si-Eumelanin Hybrids. *The Journal of Physical Chemistry C* **2018**, *122*, 28405−28415.
(23) Weickert, J.; Dunbar, R. B.; Hesse, H. C.; Wiedemann, W.; Schmidt-Mende, L. Nanostructured Organic and Hybrid Solar Cells. *Adv. Mater.* **2011**, *23*, 1810−1828.
(24) Sarna, T.; Pilas, B.; Land, E. J.; Truscott, T. Interaction of radicals from water radiolysis with melanin. *Biochimica et Biophysica Acta (BBA) - General Subjects* **1986**, *883*, 162−167.
(25) Ridente, Y.; Azzellini, G. C.; Ito, A. S. Free Radicals in Melanin-Cationic Porphyrins Complexes in the Dark and Under Light Irradiation. *Pigment Cell Research* **1993**, *6*, 134−139.
(26) Prampolini, G.; Cacelli, I.; Ferretti, A. Intermolecular interactions in eumelanins: a computational bottom-up approach. I. small building blocks. *RSC Adv.* **2015**, *5*, 38513−38526.
(27) Pezzella, A.; Iadonisi, A.; Valerio, S.; Panzella, L.; Napolitano, A.; Adinolfi, M.; d'Ischia, M. Disentangling Eumelanin "Black Chromophore": Visible Absorption Changes As Signatures of Oxidation State- and Aggregation-Dependent Dynamic Interactions in a Model Water-Soluble 5,6-Dihydroxyindole Polymer. *J. Am. Chem. Soc.* **2009**, *131*, 15270−15275.
(28) Micillo, R.; Panzella, L.; Koike, K.; Monfrecola, G.; Napolitano, A.; d' Ischia, M. "Fifty Shades" of Black and Red or How Carboxyl Groups Fine Tune Eumelanin and Pheomelanin Properties. *International Journal of Molecular Sciences* **2016**, *17*, 746.
(29) Micillo, R.; Panzella, L.; Iacomino, M.; Prampolini, G.; Cacelli, I.; Ferretti, A.; Crescenzi, O.; Koike, K.; Napolitano, A.; d'Ischia, M. Eumelanin broadband absorption develops from aggregation-modulated chromophore interactions under structural and redox control. *Scientific Reports* **2017**, *7*, No. 41532.
(30) d'Ischia, M.; Napolitano, A.; Ball, V.; Chen, C.-T.; Buehler, M. J. Polydopamine and Eumelanin: From StructureProperty Relationships to a Unified Tailoring Strategy. *Acc. Chem. Res.* **2014**, *47*, 3541−3550.
(31) Nighswander-Rempel, S. P.; Mahadevan, I. B.; Rubinsztein-Dunlop, H.; Meredith, P. Time-Resolved and Steady-State Fluorescence Spectroscopy of Eumelanin and Indolic Polymers. *Photochem. Photobiol.* **2007**, *83*, 1449−1454.
(32) Xiao, M.; Chen, W.; Li, W.; Zhao, J.; Hong, Y.-l.; Nishiyama, Y.; Miyoshi, T.; Shawkey, M. D.; Dhinojwala, A. Elucidation of the hierarchical structure of natural eumelanins. *Journal of The Royal Society Interface* **2018**, *15*, No. 20180045.
(33) Watt, A. A. R.; Bothma, J. P.; Meredith, P. The supramolecular structure of melanin. *Soft Matter* **2009**, *5*, 3754−3760.
(34) Chen, C.-T.; Ball, V.; de Almeida Gracio, J. J.; Singh, M. K.; Toniazzo, V.; Ruch, D.; Buehler, M. J. Self-Assembly of Tetramers of 5,6-Dihydroxyindole Explains the Primary Physical Properties of Eumelanin: Experiment, Simulation, and Design. *ACS Nano* **2013**, *7*, 1524−1532.
(35) Cheng, J.; Moss, S. C.; Eisner, M.; Zschack, P. X-Ray Characterization of MelaninsI. *Pigment Cell Research* **1994**, *7*, 255−262.
(36) Cheng, J.; Moss, S. C.; Eisner, M. X-Ray Characterization of MelaninsII. *Pigment Cell Research* **1994**, *7*, 263−273.
(37) Zajac, G.; Gallas, J.; Cheng, J.; Eisner, M.; Moss, S.; Alvarado-Swaisgood, A. The fundamental unit of synthetic melanin: a verification by tunneling microscopy of X-ray scattering results. *Biochimica et Biophysica Acta (BBA) - General Subjects* **1994**, *1199*, 271−278.
(38) Zajac, G. W.; Gallas, J. M.; Alvarado-Swaisgood, A. E. Tunneling microscopy verification of an x-ray scattering-derived molecular model of tyrosine-based melanin. *Journal of Vacuum Science & Technology B: Microelectronics and Nanometer Structures Processing, Measurement, and Phenomena* **1994**, *12*, 1512−1516.
(39) Díaz, P.; Gimeno, Y.; Carro, P.; González, S.; Schilardi, P. L.; Benítez, G.; Salvarezza, R. C.; Creus, A. H. Electrochemical Self-Assembly of Melanin Films on Gold. *Langmuir* **2005**, *21*, 5924−5930.
(40) Sobolewski, A. L.; Domcke, W. Photophysics of Eumelanin: Ab Initio Studies on the Electronic Spectroscopy and Photochemistry of 5,6-Dihydroxyindole. *ChemPhysChem* **2007**, *8*, 756−762.
(41) Tuna, D.; Udvarhelyi, A.; Sobolewski, A. L.; Domcke, W.; Domratcheva, T. Onset of the Electronic Absorption Spectra of


https://doi.org/10.1021/acs.jpca.3c04898
J. Phys. Chem. A 2023, 127, 10797−10806

Isolated and -Stacked Oligomers of 5,6-Dihydroxyindole: An Ab Initio Study of the Building Blocks of Eumelanin. *The Journal of Physical Chemistry B* **2016**, *120*, 3493−3502.
(42) Datar, A.; Hazra, A. Pathways for Excited-State Nonradiative Decay of 5,6-Dihydroxyindole, a Building Block of Eumelanin. *The Journal of Physical Chemistry A* **2017**, *121*, 2790−2797.
(43) Ghosh, P.; Ghosh, D. Effect of Dimerization on the Nonradiative Processes of Eumelanin Monomer. *The Journal of Physical Chemistry B* **2021**, *125*, 547−556.
(44) Ghosh, P.; Ghosh, D. Elucidating the Photoprotection Mechanism of Eumelanin Monomers. *The Journal of Physical Chemistry B* **2017**, *121*, 5988−5994.
(45) Kaxiras, E.; Tsolakidis, A.; Zonios, G.; Meng, S. Structural Model of Eumelanin. *Phys. Rev. Lett.* **2006**, *97*, No. 218102.
(46) Meng, S.; Kaxiras, E. Theoretical Models of Eumelanin Protomolecules and their Optical Properties. *Biophys. J.* **2008**, *94*, 2095−2105.
(47) Pinna, E.; Melis, C.; Antidormi, A.; Cardia, R.; Sechi, E.; Cappellini, G.; d'Ischia, M.; Colombo, L.; Mula, G. Deciphering Molecular Mechanisms of Interface Buildup and Stability in Porous Si/Eumelanin Hybrids. *International Journal of Molecular Sciences* **2017**, *18*, 1567.
(48) Frisch, M. J.; Trucks, G. W.; Schlegel, H. B.; Scuseria, G. E.; Robb, M. A.; Cheeseman, J. R.; Scalmani, G.; Barone, V.; Petersson, G. A.; Nakatsuji, H.; Li, X.; Caricato, M.; Marenich, A. V.; Bloino, J.; Janesko, B. G.; Gomperts, R.; Mennucci, B.; Hratchian, H. P.; Ortiz, J. V.; Izmaylov, A. F.; Sonnenberg, J. L.; Williams-Young, D.; Ding, F.; Lipparini, F.; Egidi, F.; Goings, J.; Peng, B.; Petrone, A.; Henderson, T.; Ranasinghe, D.; Zakrzewski, V. G.; Gao, J.; Rega, N.; Zheng, G.; Liang, W.; Hada, M.; Ehara, M.; Toyota, K.; Fukuda, R.; Hasegawa, J.; Ishida, M.; Nakajima, T.; Honda, Y.; Kitao, O.; Nakai, H.; Vreven, T.; Throssell, K.; Montgomery, J. A., Jr.; Peralta, J. E.; Ogliaro, F.; Bearpark, M. J.; Heyd, J. J.; Brothers, E. N.; Kudin, K. N.; Staroverov, V. N.; Keith, T. A.; Kobayashi, R.; Normand, J.; Raghavachari, K.; Rendell, A. P.; Burant, J. C.; Iyengar, S. S.; Tomasi, J.; Cossi, M.; Millam, J. M.; Klene, M.; Adamo, C.; Cammi, R.; Ochterski, J. W.; Martin, R. L.; Morokuma, K.; Farkas, O.; Foresman, J. B.; Fox, D. J. *Gaussian 16*, rev. B.01; Gaussian Inc. Wallingford CT, 2016.
(49) Zhao, Y.; Truhlar, D. G. A new local density functional for main-group thermochemistry, transition metal bonding, thermochemical kinetics, and noncovalent interactions. *The Journal of Chemical Physics* **2006**, *125*, No. 194101.
(50) Zhao, Y.; Truhlar, D. G. The M06 suite of density functionals for main group thermochemistry, thermochemical kinetics, noncovalent interactions, excited states, and transition elements: two new functionals and systematic testing of four M06-class functionals and 12 other functionals. *Theor. Chem. Acc.* **2008**, *120*, 215−241.
(51) Papajak, E.; Leverentz, H. R.; Zheng, J.; Truhlar, D. G. Efficient Diffuse Basis Sets: cc-pVxZ+ and maug-cc-pVxZ. *Journal of Chemical Theory and Computation* **2009**, *5*, 1197−1202.
(52) Schlegel, H. B. Optimization of equilibrium geometries and transition structures. *J. Comput. Chem.* **1982**, *3*, 214−218.
(53) Malloci, G.; Cappellini, G.; Mulas, G.; Mattoni, A. A (time dependent) density functional theory study of the optoelectronic properties of bis-triisopropylsilylethynyl functionalized acenes. *Thin Solid Films* **2013**, *543*, 32−34.
(54) Malloci, G.; Mulas, G.; Cappellini, G.; Joblin, C. Time-dependent density functional study of the electronic spectra of oligoacenes in the charge states −1, 0, + 1, and + 2. *Chem. Phys.* **2007**, *340*, 43−58.
(55) Malloci, G.; Cappellini, G.; Mulas, G.; Mattoni, A. Electronic and optical properties of families of polycyclic aromatic hydrocarbons: A systematic (time-dependent) density functional theory study. *Chem. Phys.* **2011**, *384*, 19−27.
(56) Cardia, R.; Malloci, G.; Mattoni, A.; Cappellini, G. Effects of TIPS-Functionalization and Perhalogenation on the Electronic, Optical, and Transport Properties of Angular and Compact Dibenzochrysene. *The Journal of Physical Chemistry A* **2014**, *118*, 5170−5177.
(57) Cardia, R.; Malloci, G.; Rignanese, G.-M.; Blase, X.; Molteni, E.; Cappellini, G. Electronic and optical properties of hexathiapentacene in the gas and crystal phases. *Phys. Rev. B* **2016**, *93*, No. 235132.
(58) Cardia, R.; Malloci, G.; Bosin, A.; Serra, G.; Cappellini, G. Computational investigation of the effects of perfluorination on the charge-transport properties of polyaromatic hydrocarbons. *Chem. Phys.* **2016**, *478*, 8−13. Charge Carrier Dynamics at the Nanoscale
(59) Cardia, R.; Malloci, G.; Serra, G.; Bosin, A.; Cappellini, G. Electronic and optical properties of functionalized polyaromatic hydrocarbons: a computational investigation on perfluorinated circumacenes. *Proceedings Vol. 9895 SPIE Photonics Europe Conference* **2016**, 63−70. Organic Photonics VII 3−7 APRIL 2016.
(60) Dardenne, N.; Cardia, R.; Li, J.; Malloci, G.; Cappellini, G.; Blase, X.; Charlier, J.-C.; Rignanese, G.-M. Tuning Optical Properties of Dibenzochrysenes by Functionalization: A Many-Body Perturbation Theory Study. *The Journal of Physical Chemistry C* **2017**, *121*, 24480−24488.
(61) Kumar, A.; Cardia, R.; Cappellini, G. Electronic and optical properties of chromophores from bacterial cellulose. *Cellulose* **2018**, *25*, 2191−2203.
(62) Mocci, P.; Cardia, R.; Cappellini, G. Inclusions of Si-atoms in Graphene nanostructures: a computational study on the ground-state electronic properties of Coronene and Ovalene. *Journal of Physics* **2018**, *956*, No. 012020.
(63) Mocci, P.; Cardia, R.; Cappellini, G. Si-atoms substitutions effects on the electronic and optical properties of coronene and ovalene. *New Journal of Physics* **2018**, *20*, No. 113008.
(64) Mocci, P.; Cardia, R.; Cappellini, G. A computational study on the electronic and optical properties of boron-nitride circumacenes. *Phys. Chem. Chem. Phys.* **2019**, *21*, 16302−16309.
(65) Becke, A. D. Density-functional thermochemistry. III. The role of exact exchange. *J. Chem. Phys.* **1993**, *98*, 5648.
(66) Lee, C.; Yang, W.; Parr, R. G. Development of the Colle-Salvetti correlation-energy formula into a functional of the electron density. *Phys. Rev. B* **1988**, *37*, 785−789.
(67) Ditchfield, R.; Hehre, W. J.; Pople, J. A. Self-Consistent Molecular-Orbital Methods. IX. An Extended Gaussian-Type Basis for Molecular-Orbital Studies of Organic Molecules. *The Journal of Chemical Physics* **1971**, *54*, 724−728.
(68) Molteni, E.; Cappellini, G.; Cardia, R.; Onida, G.; Mula, G. Eumelanin Adsorption on Silicon: Optical Properties of Si(001)-Adsorbed Eumelanin Tetrameric Protomolecules. *The Journal of Physical Chemistry C* **2020**, *124*, 9376−9384.
(69) Casida, M. E. *Recent Advances in Density Functional Methods*; World Scientific Publishing, 1995; Chapter 5, pp 155−192.
(70) Tomasi, J.; Mennucci, B.; Cammi, R. Quantum Mechanical Continuum Solvation Models. *Chemical Reviews* **2005**, *105*, 2999−3094.
(71) Marenich, A. V.; Cramer, C. J.; Truhlar, D. G. Universal Solvation Model Based on Solute Electron Density and on a Continuum Model of the Solvent Defined by the Bulk Dielectric Constant and Atomic Surface Tensions. *The Journal of Physical Chemistry B* **2009**, *113*, 6378−6396.
(72) Ghosh, P.; Ghosh, D. Effect of microsolvation on the non-radiative decay of the eumelanin monomer. *Phys. Chem. Chem. Phys.* **2019**, *21*, 26123−26132.
(73) Karsili, T. N. V.; Marchetti, B.; Matsika, S. Origins of Photodamage in Pheomelanin Constituents: Photochemistry of 4-Hydroxybenzothiazole. *The Journal of Physical Chemistry A* **2018**, *122*, 1986−1993.
(74) Onida, G.; Reining, L.; Rubio, A. Electronic excitations: density-functional versus many-body Green's-function approaches. *Rev. Mod. Phys.* **2002**, *74*, 601−659.
(75) Cappellini, G.; Furthmüller, J.; Cadelano, E.; Bechstedt, F. Electronic and optical properties of cadmium fluoride: The role of many-body effects. *Physical Review B* **2013**, *87*, 075203 DOI: 10.1103/PhysRevB.87.075203.
(76) Sangalli, D.; Ferretti, A.; Miranda, H.; Attaccalite, C.; Marri, I.; Cannuccia, E.; Melo, P.; Marsili, M.; Paleari, F.; Marrazzo, A.; et al.

Many-body perturbation theory calculations using the yambo code. *Journal of Physics: Condensed Matter* **2019**, *31*, No. 325902.
(77) Blase, X.; Duchemin, I.; Jacquemin, D. The Bethe-Salpeter equation in chemistry: relations with TD-DFT, applications and challenges. *Chem. Soc. Rev.* **2018**, *47*, 1022−1043.
(78) Blase, X.; Duchemin, I.; Jacquemin, D.; Loos, P.-F. The Bethe-Salpeter Equation Formalism: From Physics to Chemistry. *The Journal of Physical Chemistry Letters* **2020**, *11* (17), 7371−7382.
(79) Blase, X.; Attaccalite, C.; Olevano, V. First-principles GW calculations for fullerenes, porphyrins, phtalocyanine, and other molecules of interest for organic photovoltaic applications. *Phys. Rev. B* **2011**, *83*, No. 115103.
(80) Blase, X.; Attaccalite, C. Charge-transfer excitations in molecular donor-acceptor complexes within the many-body Bethe-Salpeter approach. *Appl. Phys. Lett.* **2011**, *99*, No. 171909.
(81) Jacquemin, D.; Duchemin, I.; Blase, X. Benchmarking the Bethe-Salpeter Formalism on a Standard Organic Molecular Set. *J. Chem. Theory Comput.* **2015**, *11*, 3290−3304.
(82) Loos, P.-F.; Scemama, A.; Duchemin, I.; Jacquemin, D.; Blase, X. Pros and Cons of the BetheSalpeter Formalism for Ground-State Energies. *The Journal of Physical Chemistry Letters* **2020**, *11*, 3536−3545.
(83) Assis Oliveira, L. B.; Fonseca, T. L.; Costa Cabral, B. J.; Coutinho, K.; Canuto, S. Hydration effects on the electronic properties of eumelanin building blocks. *The Journal of Chemical Physics* **2016**, *145*, No. 084501.
(84) Duchemin, I.; Deutsch, T.; Blase, X. Short-Range to Long-Range Charge-Transfer Excitations in the Zincbacteriochlorin-Bacteriochlorin Complex: A Bethe-Salpeter Study. *Phys. Rev. Lett.* **2012**, *109*, No. 167801.
(85) Boulanger, P.; Jacquemin, D.; Duchemin, I.; Blase, X. Fast and Accurate Electronic Excitations in Cyanines with the Many-Body Bethe-Salpeter Approach. *Journal of Chemical Theory and Computation* **2014**, *10*, 1212−1218.
(86) Le Guennic, B.; Jacquemin, D. Taking Up the Cyanine Challenge with Quantum Tools. *Acc. Chem. Res.* **2015**, *48*, 530−537.
(87) Faber, C.; Duchemin, I.; Deutsch, T.; Blase, X. Many-body Green's function study of coumarins for dye-sensitized solar cells. *Phys. Rev. B* **2012**, *86*, 155315.
(88) Palummo, M.; Hogan, C.; Sottile, F.; Bagalá, P.; Rubio, A. Ab initio electronic and optical spectra of free-base porphyrins: The role of electronic correlation. *The Journal of Chemical Physics* **2009**, *131*, No. 084102.
(89) Assis Oliveira, L. B.; Fonseca, T. L.; Cabral, B. J. C.; Coutinho, K.; Canuto, S. Preferential solvation and optical properties of eumelanin building blocks in binary mixture of methanol and water. *The Journal of Chemical Physics* **2021**, *155*, No. 174504.
(90) Ljungberg, M. P.; Koval, P.; Ferrari, F.; Foerster, D.; Sánchez-Portal, D. Cubic-scaling iterative solution of the Bethe-Salpeter equation for finite systems. *Phys. Rev. B* **2015**, *92*, No. 075422.
(91) Malcıoğlu, O. B.; Calzolari, A.; Gebauer, R.; Varsano, D.; Baroni, S. Dielectric and Thermal Effects on the Optical Properties of Natural Dyes: A Case Study on Solvated Cyanin. *J. Am. Chem. Soc.* **2011**, *133*, 15425−15433.
(92) Cudazzo, P.; Gatti, M.; Rubio, A.; Sottile, F. Frenkel versus charge-transfer exciton dispersion in molecular crystals. *Phys. Rev. B* **2013**, *88*, No. 195152.



https://doi.org/10.1021/acs.jpca.3c04898
*J. Phys. Chem. A* 2023, 127, 10797−10806